AERODYNAMIC DANCER IN WEB HANDLING

by

E. Y. Hong, J. J. Shelton, and Y. B. Chang
Oklahoma State University
USA

ABSTRACT

This paper discusses the aerodynamic dancer that is effective in a wide range of frequency and do not cause excessive lateral web deflection, touching, or flutter. An aerodynamic model of air-turn bar has been developed. The model can handle air-turn bars that have varying density of air-emitting holes. The model predicts the average flotation height of the web, cushion pressure profile under the web, and the rate of air consumption for given operating conditions. Experimental verification of the aerodynamic model has been done with a stationary-web test setup. The air gap profile, the cushion pressure profile, and the air consumption were measured, and the results were compared with the prediction. Also examined was the possibility of using an air reverser for determination of web tension. Web tension was varied up to 175 N/m (1.5 lbf/in). The measurement error of web tension based on cushion pressure was less than 5 percent in the entire range of test conditions. An air dancer model has been developed based on the aerodynamic model of air-turn bars and compared with experimental results. It was shown that the air dancer system has a much wider useful frequency range compared to the conventional dancer system.

INTRODUCTION

Dancers are commonly used in web handling process lines to attenuate web tension fluctuations caused by eccentric rollers, uneven wound rolls, misalignment of idle rollers, and other disturbances. The position of a dancer is also used as a tension feedback control system. It is very important to regulate the undesired tension variations within the desired limits to have a good quality printing and not to cause web breakage or wrinkling. A conventional dancer consists of a roller supported by a mechanical system such as a spring or pneumatic actuator.

The performance of a dancer as a positioner for control of the velocity of a web transport element, or of a load-cell transducer for the measurement of tension, is limited by the rotational inertia of the roller as dictated by the required ruggedness. Furthermore, the dynamic behavior above a certain frequency is unpredictable because of the

uncertainty of dynamic slippage between the web and the roller. Even in a laboratory environment, the measurement of dynamic tension may be spurious.

One way to eliminate rotational inertia and the uncertainty of web-to-roller slippage of dancer and load-cell systems is to use aerodynamic support devices. Expected characteristics and benefits of an aerodynamic system include that there is no rotating component, there is no tension variation between the incoming and outgoing spans, and the supporting device can be much lighter than conventional rollers for improved frequency response to the tension disturbances. Air support devices, however, can cause undesirable effects such as excessive lateral deflection of the web, touch-down, and flutter. It is desirable to develop an air dancer and tension transducer system which performs better than conventional dancers and conventional tension load cells without the adverse effects that some air support devices have.

AERODYNAMIC MODELING OF AN AIR-TURN BAR

Consider the air flow ejected from the holes of an air-turn bar and flowing through the gap under the web, as shown in Figure 1. The cross section of the system is shown in Figure 2.

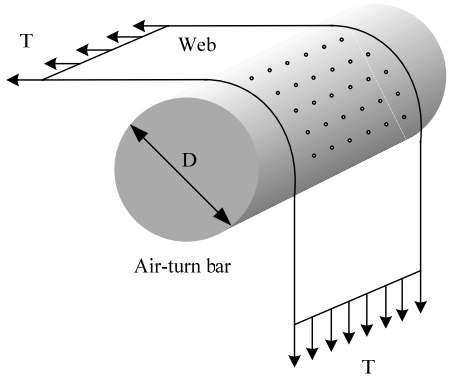

Figure 1 – Schematic view of web supported by air-turn bar

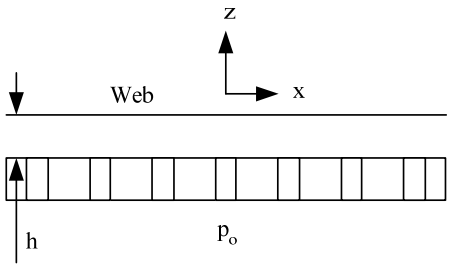

Figure 2 – Cross section of web and air-turn bar

The air gap is assumed to be so much smaller than other geometric dimensions that the velocity in the z-direction is neglected in this study. The gap is assumed constant. The air-emitting hole distribution over the air-turn bar is described as a parameter, α, based on the opening area over a per unit surface area of the air-turn bar. Overall hole patterns are shown in Figure 3 and the detail of the hole distributions is shown in Figure 4. For example, the density of holes in the edge section can be written as $\alpha_2 = \frac{3}{4}\pi r^2 / b_2 c_2$. In the same way, the hole densities for the other sections can be found as $\alpha_1 = \frac{1}{2}\pi r^2 / b_1 c_1$ and $\alpha_o = \pi r^2 / b_o c_o$.

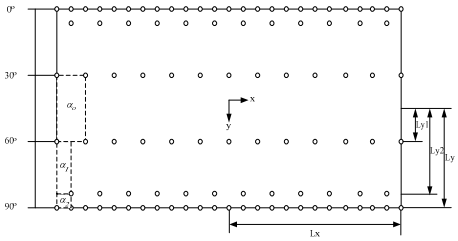

Figure 3 – Hole distribution over air- turn bar

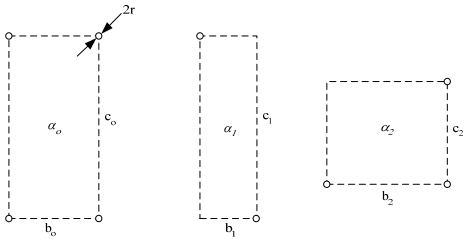

Figure 4 – Detail of hole pattern

The flow field over the gap between the web and the air-turn bar can be described by the mass conservation equation and the momentum equation. It is assumed that the flow incompressible.

$$\frac{\partial h}{\partial t}+\frac{\partial (hu)}{\partial x}+\frac{\partial (hv)}{\partial y}=\alpha U \qquad \{1\}$$

$$\rho\frac{\partial u}{\partial t}+\rho u\frac{\partial u}{\partial x}+\rho v\frac{\partial u}{\partial y}+\frac{\partial p}{\partial x}=\mu(\frac{\partial^2 u}{\partial x^2}+\frac{\partial^2 u}{\partial y^2})-\alpha\rho U\frac{u}{h} \qquad \{2\}$$

$$\rho\frac{\partial v}{\partial t}+\rho u\frac{\partial v}{\partial x}+\rho v\frac{\partial v}{\partial y}+\frac{\partial p}{\partial y}=\mu(\frac{\partial^2 v}{\partial x^2}+\frac{\partial^2 v}{\partial y^2})-\alpha\rho U\frac{v}{h} \qquad \{3\}$$

The effect of viscosity on pressure distributions under the web is neglected. It is believed that more accurate results can be obtained by including viscous effects on the flow field. It is true that along the center line, in either x or y direction, the flow can be one dimensional. Based on all these assumptions, the steady-state governing equation of equation {1}, {2}, and {3} can be written as

$$\frac{du}{dx}=\frac{\alpha U}{h} \qquad \{4\}$$

$$\frac{dp}{dx}+\rho u\frac{du}{dx}+\frac{\rho\alpha U}{h}u=0 \qquad \{5\}$$

and

$$\frac{dv}{dy}=\frac{\alpha U}{h} \qquad \{6\}$$

$$\frac{dp}{dy}+\rho v\frac{dv}{dy}+\frac{\rho\alpha U}{h}v=0 \qquad \{7\}$$

An average velocity through a hole of the air-turn bar can be calculated as

$$U = C\sqrt{\frac{2(p_o - p)}{\rho}} = CU_o\sqrt{1 - \frac{p}{p_o}} \quad \{8\}$$

where C is the discharge coefficient which is 0.72 (Tang, 2003), and

$$U_o = \sqrt{2\frac{p_o}{\rho}} \quad \{9\}$$

Refer to the detail procedure to obtain the solutions (Hong, 2005). The closed form solution for the pressure profile in the middle section in two dimensions might be written as

$$p(x,y) = p_o\left[1 - \left(\frac{e^{\beta_o x} + e^{-\beta_o x}}{e^{L_x\beta_o} + e^{-L_x\beta_o}}\right)^2\right]\left[1 - \left[\frac{\sqrt{2}}{U_o}\left(C_6 e^{\beta_o y} - C_5 e^{-\beta_o y}\right)\right]^2\right]$$

$$\left[-L_x \le x \le L_x\right] \textit{ and } \left[-L_{y1} \le x \le L_{y1}\right] \quad \{10\}$$

where $\beta_o = \sqrt{2}\frac{C\alpha_o}{h}$.

Tension per unit width of the web can be obtained by the following relationship:

$$T = \frac{D}{2}\frac{\int_{-L_x}^{L_x} p(x,0)dx}{2L_x} \quad \{11\}$$

$$= \frac{p_o D}{4L_x}\left[1 - \left[\frac{\sqrt{2}}{U_o}(C_6 - C_5)\right]^2\right]\left[2L_x - \frac{4L_x + \frac{e^{2L_x\beta_o} - e^{-2L_x\beta_o}}{\beta_o}}{(e^{L_x\beta_o} - e^{-L_x\beta_o})^2}\right] \quad \{12\}$$

Equation {8} can be rewritten as

$$U(x,y) = C\sqrt{\frac{2(p_o - p)}{\rho}} = CU_o\sqrt{1 - \frac{p}{p_o}} = CU_o\sqrt{1 - \frac{p(x,y)}{p_o}} \quad \{13\}$$

where C is the discharge coefficient which is 0.72, and

$$U_o = \sqrt{2\frac{p_o}{\rho}} \quad \{14\}$$

Volume flow rate of the web can be calculated as

$$Q = 4(\alpha_o \int_0^{L_x} \int_0^{L_{y1}} U(x,y)dxdy + \alpha_1 \int_0^{L_x} \int_{L_{y1}}^{L_{y2}} U(x,y)dxdy + \alpha_2 \int_0^{L_x} \int_{L_{y2}}^{L_y} U(x,y)dxdy) \quad \{15\}$$

The effect of supply pressure into the air-turn bar on pressure profile is shown in Figure 5. The pressure profile becomes more uniform in the center region along the cross machine direction of the web when the supply pressure is lower, when the web tension is higher, and when the web is wider. The flotation height increases with the size of emitting holes, but it does not strongly affect the pressure profile. The effect of tension and the supply pressure on flotation height is shown in Figure 7. The flotation height increases when the tension becomes lower as expected. Note that a higher supply pressure allows a wider range of web tension. The limitation of web tension can be found for each supply pressure. Figure 6 shows the relationship between the web tension and the pressure calculated at the center region of the air-turn bar under the web. It is found that the web tension has a very linear relationship with the center pressure of the air-turn bar under the web. Therefore, the web tension can be found simply by multiplying a tension factor (a slope = 34.7 for these operating and geometric conditions) to the center pressure. This method can be used in measuring the web tension without physical contacts. It was used to measure the web tension in the dynamic situations and compared with conventional method using load cells.

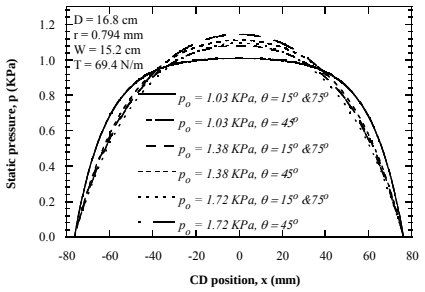

Figure 5 – Effect of supply pressure on pressure profile

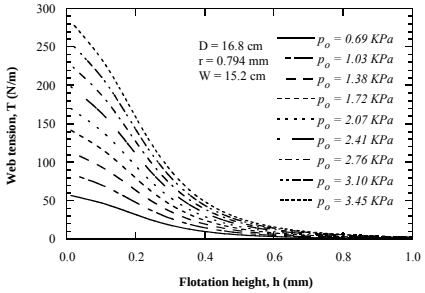

Figure 7 – Effect of web tension and supply pressure on flotation height

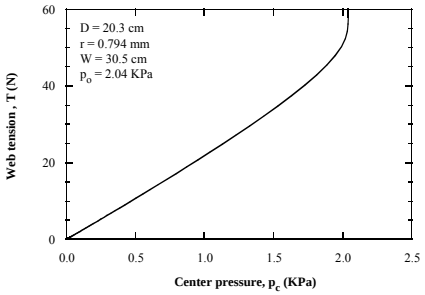

Figure 6 – Relationship between web tension and center pressure

Experiments

The test setup consisted of two air-turn bars, a steel frame, a flexible web (plastic film), a flow meter, and instruments including a pressure transducer and a displacement

laser sensor. These air-turn bars were made of 16.83-centimeter (6.625-inch) diameter aluminum cylinders and have multiple pressure taps for measurements of pressure variation in the cross machine direction and along the circumference of the air-turn bar as shown in Figure 8. A 6-inch-wide, stationary, horizontal span of web was supported by the air-turn bars. The thickness of the web was 0.0672 mm (0.003 inches). To apply tension on the web, two identical weights were attached at the two ends of the web. The weights were placed on a plate which was fixed with a vertical rod and a string to each end of the web as shown in Figure 9. A laser displacement meter (Keyence, Model No. LC-2210) was mounted on the air-turn bar with a sliding linear guide to measure the out-of-plane deflections of the web across the air-turn bar at selected points. A flow meter (Rotameter, Omega, FL - 401A) was installed at the upstream of the air-turn bar to measure the supplied flow rate into the air-turn bar. To measure the pressure distribution on the web, a pressure transducer (Validyne, Model No. DP15-32) and a carrier demodulator (Validyne, Model No. CD15) were used. The pressure transducer had a maximum range of 13.7 KPa (55.0 inches of water or 2.0 psi) with a resolution 34.2 Pa (0.1375 inches of water or 0.005 psi). The carrier yielded a DC voltage output, which was then fed into a digital data acquisition system.

Before the test was conducted, the pressure transducer was calibrated against a vertical tube manometer in the range of 0 to 4.98 KPa (20 inches of water). The laser displacement meter does not require any calibration, although validity of read-out of the laser displacement sensor was checked. A calibration sheet was provided for flow meter readings by the manufacturer. The two air-turn bars were aligned carefully so that the web met them perpendicularly. After two identical weights were placed at the each end of the web to tension the web, the air-turn bars were pressurized at a predetermined value. To stabilize the web laterally, the web was affixed in the middle with tape on the structure of the test setup. At a certain test condition, the pressure distributions were measured using the data acquisition system, the flying flotation heights of the web were measured by the laser displacement meter, the flow rate supplied into the air-turn bar was measured by the flow meter, and the plenum pressure (supplied air pressure into the air-turn bar) was measured by the vertical manometer. The main test parameters were the air supply pressure inside the air-turn bar and the web tension. The geometric conditions such as diameter of the air-turn bar, the air emitting-hole size, and the hole-pattern were not varied. The values of the test parameters are tabulated in Table 1.

Parameter	Symbol	Value
Diameter of air-turn bar	D	16.83 cm (6.625 inches)
Radius of air-emitting hole	r	0.794 mm (1/32 inches)
Web width	W	15.2 cm (6 inches)
Web tension	T	25.6 – 244 N/m (0.146 - 1.396 lbf/in)
Supply pressure	p_o	0.361 – 3.74 Kpa (0.0524 - 0.542 psig)

Table 1 – Air-turn bar test conditions

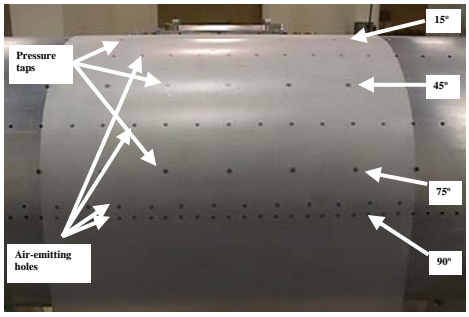

Figure 8 – Detail view of air-turn bar

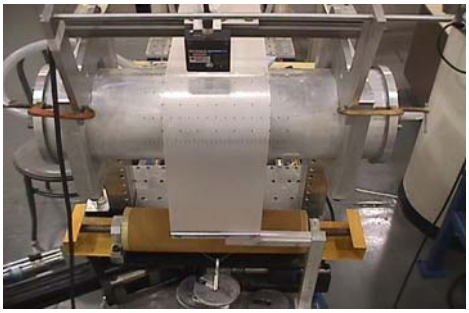

Figure 9 – Flotation height measurements

Comparisons

Comparing the results from the analytical model with the experimental data showed a generally strong agreement. Figure 10 and Figure 13 show the comparison of the pressure profile under the web between the experimental data and the results from the analytical model. They are compared in the range of 26.3 N/m (0.15 lbf/in) to 263 N/m (1.5 lbf/in) in the web tension and 345 Pa (0.05 psi) to 3450 Pa (0.5 psi) in the air supply pressure. The predicted pressure profiles tend to agree better with the experimental data at higher flow rates and higher supply pressures. The comparison of the applied web tension and the measured web tension is shown in Figure 11. The measured web tension was obtained by multiplying the average cushion pressure between the air-turn bar and the web by the radius of the air-turn bar. The measured web tensions deviated more with higher web tensions. The deviation was less than 5 % throughout all the test conditions, up to 263 N/m (1.5 lbf/in) of web tension. This comparison shows the feasibility of air devices to measure the web tension in the web process line. The experimental data for the flotation height were compared with the results from the analytical model in Figure 14. As shown in Figure 14, comparisons of the results from the analytical model with experimental data showed agreement for higher flotation heights, namely for lower web tensions. The discrepancy between the predicted and measured flotation heights appear to be larger with increased web tensions. It might be due to the viscosity of the air. When the web tensions are high, the flotation heights from the analytical model were predicted to be higher than those from the experiments. Figure 12 shows comparisons of the effect of supply pressure on flotation heights. Note that the experimental data for the flotation heights are average values of flotation heights over the entire measurements at a certain web tension and air supply pressure. This figure summarizes comparisons of experimental data with the flotation heights from the analytical model for the whole range of tests in one graph. As the web tensions were increased, the analytical model over predicted.

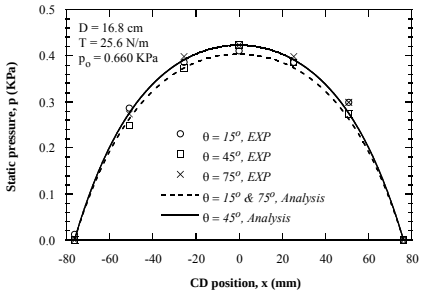

Figure 10 – Comparison of pressure distributions under the web (T = 25.6 N/m and p_o = 0.660 KPa)

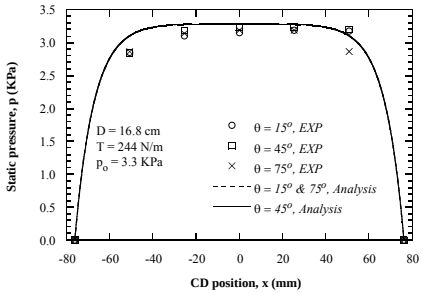

Figure 13 – Comparison of pressure distributions under the web (T = 244 N/m and p_o = 3.3 KPa)

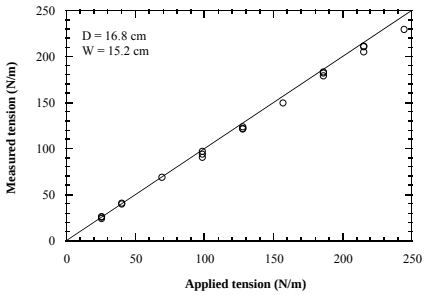

Figure 11 – Verification of non-contact tension measurements

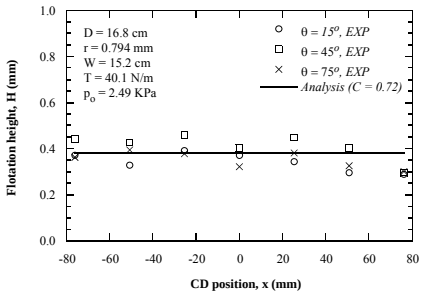

Figure 14 – Comparison of flotation height over air-turn bar (T = 40.1 N/m and p_o = 2.49 KPa)

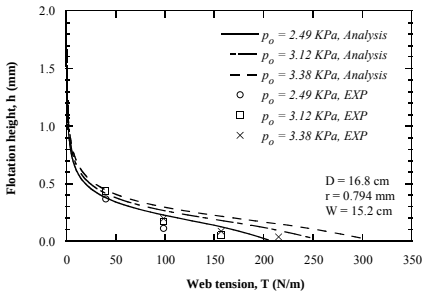

Figure 12 – Comparison of effect of supply pressure on flotation height (C= 0.72)

DYNAMIC MODELING OF AN AIR DANCER

Theoretical Analyses

A schematic of the air-dancer is shown in Figure 15. The web is traveling from left to right. It is considered that the upstream velocity, V_o, changes because of an angular-velocity-controlled unwinder.

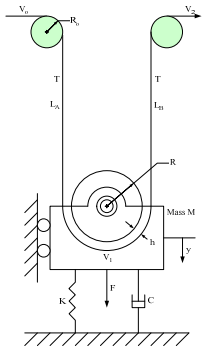

Figure 15 – Schematic of air-dancer

The dynamic continuity equation for a span can be expressed by equations {16} and {17}. The difference between the length of web entering the span and the length of web leaving the span in a certain period of time is the same as the accumulation of length in the span.

For A span,

$$\frac{V_o}{1+\varepsilon_o}dt - \frac{V_1}{1+\varepsilon_A}dt = d\left[\frac{L_A + \frac{\pi(R+h)}{2}}{1+\varepsilon_A}\right] \qquad \{16\}$$

For B span,

$$\frac{V_1}{1+\varepsilon_A}dt - \frac{V_2}{1+\varepsilon_B}dt = d\left[\frac{L_B + \frac{\pi(R+h)}{2}}{1+\varepsilon_B}\right] \qquad \{17\}$$

where $\varepsilon_A = \varepsilon_B = \dfrac{T}{EtW}$.

As shown in Figure 16, the relationship between the web tension and the flotation height of the web over an air-dancer may be simply linearized except for the extremely low tension (extremely high air gap) and high tension (extremely low air gap). The linear curve with an air damping effect can be written as

$$T = K_{air}(H_o - h) + C_{air}\frac{d}{dt}(H_o - h) \qquad \{18\}$$

where $C_{air} \cong \frac{\mu(\pi R)W^3}{4h^3}$ for three dimensional squeeze film effects ($C_{air} = \frac{\mu(\pi R)W^3}{2h^3}$ for two dimensional squeeze film effects - Blevins, 1992).

The linear approximation can represent the relationship between the web tension and the flotation height of the web fairly well for operating ranges of web tension from 17.8 N (4 lbf) to 66.7 N (15 lbf) for the given design, web width (30.5 cm or 12 inches), and supply pressure (2.04 Kpa or 0.296 psig). K_{air} = 174 KN/m (996 lbf/in) and C_{air} = 3.28 KN-s/m (18.7 lbf-s/in) were used for this geometric and operational conditions in this study. Notice that the operating range of web tension can be much larger with a large width of the web and a higher supply pressure.

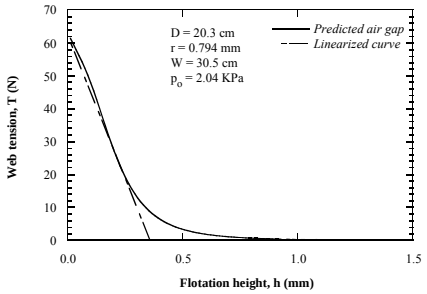

Figure 16 – Simple linearization of relationship between web tension and flotation height

If the wrap angle is 180 degrees, then the dynamic equation for linear acceleration can be expressed as

$$F - Ky - C\frac{dy}{dt} - 2T = M\frac{d^2y}{dt^2} \qquad \{19\}$$

The system of equations can be linear if the mechanical damping, C , and the spring rate, K , are constants.

The relationship of angular and linear velocity can be expressed as

$$V_o = \omega R_o \qquad \{20\}$$

An angular acceleration of the rollers can expressed as

$$(T - T_o)R_o - J_o\frac{d\omega_o}{dt} = 0 \qquad \{21\}$$

and

$$(T_2 - T)R_o - J_2\frac{d\omega_2}{dt} = 0 \qquad \{22\}$$

Note that there is no dynamic angular acceleration of the dancer because tensions between the two spans are assumed to be the same, because there is no friction between the web and the dancer. Refer to the detail procedure to obtain the equations of system (Hong, 2005). Equations of system can be expressed in matrix form:

$$\begin{bmatrix} 1 & 0 & 0 & 0 \\ -1 & 1 & \dfrac{-s(L_A+\frac{\pi}{2}H_o-\frac{\pi T}{2K_{air}}+\frac{\pi R}{2}+\frac{\pi}{2}\frac{EtW}{(C_{air}s+K_{air})})}{EtW}-\dfrac{V_1}{EtW} & s \\ 0 & -1 & \dfrac{-s(L_B+\frac{\pi}{2}H_o-\frac{\pi T}{2K_{air}}+\frac{\pi R}{2}+\frac{\pi}{2}\frac{EtW}{(C_{air}s+K_{air})})}{EtW}-\dfrac{V_2}{EtW}+\dfrac{V_1}{EtW} & s \\ 0 & 0 & 2 & Ms^2+Cs+K \end{bmatrix} \begin{bmatrix} \Delta V_o(s) \\ \Delta V_1(s) \\ \Delta T(s) \\ \Delta y(s) \end{bmatrix} = \begin{bmatrix} R_o\Delta\omega_o(s) \\ -\dfrac{V_o}{EtW}\Delta T_o(s) \\ -\Delta V_2(s) \\ \Delta F(s) \end{bmatrix} \qquad \{23\}$$

The transfer functions were obtained by the solutions of equation {23} with assumptions of $K=0$ and $C=0$, and all initial velocities were assumed to be equal for simplicity.

$$\frac{\Delta T(s)}{\Delta V_o(s)} = \frac{-\frac{M}{4}C_{air}s^2-\frac{M}{4}K_{air}s}{\frac{MC_{air}(L_A+L_B+\pi(H_o+R-\frac{T}{K_{air}}))}{4EtW}s^3+\frac{M[K_{air}(L_A+L_B+\pi(H_o+R-\frac{T}{K_{air}}))+V_1C_{air}+\pi EtW]}{4EtW}s^2+\frac{MV_1K_{air}+4EtWC_{air}}{4EtW}s+K_{air}} \qquad \{24\}$$

and

$$\frac{\Delta y(s)}{\Delta V_o(s)} = \frac{\frac{M}{2}C_{air}s^2+\frac{M}{2}K_{air}s}{s\left[\frac{MC_{air}(L_A+L_B+\pi(H_o+R-\frac{T}{K_{air}}))}{4EtW}s^3+\frac{M[K_{air}(L_A+L_B+\pi(H_o+R-\frac{T}{K_{air}}))+V_1C_{air}+\pi EtW]}{4EtW}s^2+\frac{MV_1K_{air}+4EtWC_{air}}{4EtW}s+K_{air}\right]} \qquad \{25\}$$

with a winder and unwinder differing by no more than an overall sign.

The transfer functions can be obtained by ignoring the air damping effect, yet still with the assumptions of $K=0$ and $C=0$, and all initial velocities were assumed to be equal.

$$\frac{\Delta T(s)}{\Delta V_o(s)} = \frac{-\frac{M}{4}s}{\frac{M(L_A+L_B+\pi(H_o+R-\frac{T}{K_{air}}+\frac{EtW}{K_{air}}))}{4EtW}s^2+\frac{MV_1}{4EtW}s+1} \qquad \{26\}$$

and

$$\frac{\Delta y(s)}{\Delta V_o(s)} = \frac{\frac{1}{2}}{s\left(\frac{M\left(L_A + L_B + \pi\left(H_o + R - \frac{T}{K_{air}} + \frac{EtW}{K_{air}}\right)\right)}{4EtW} s^2 + \frac{MV_1}{4EtW} s + 1\right)} \qquad \{27\}$$

with a winder and unwinder differing by no more than an overall sign.

Figure 17 shows the frequency responses of the web tension to the velocity disturbance with different masses. Magnitudes of the resonant peaks are about the same, but the effect of the mass is significant in the resonant frequency of the system. The dancer system with less mass can perform well in a much higher range of the tension disturbance. Note that the dancer system can do more harm than good near and at the resonant frequency of the tension disturbance; in that case, it is better not to have the dancer system at all in the web line. Figure 18 shows the frequency responses of the web tension to the velocity disturbance with different lengths of the web span over the dancer. Magnitudes of the resonant peaks are about the same, but the effect of the length of the web span is significant in the resonant frequency of the system. The dancer system with shorter span length can perform well in a much higher range of the tension disturbance. Note again that the dancer system can do more harm than good near and at the resonant frequency of the tension disturbance. Furthermore, the frequency response of a tension control system which uses dancer position as the tension transducer is limited to lower values than the resonant frequency of the system (Shelton, 1997). Figure 19 shows the frequency responses of the web tension to the velocity disturbance with different stiffness of the air cushion. Magnitudes of the resonant peaks are about the same, and the effect of the stiffness of the air cushion is also not very significant in terms of the resonant frequency of the system. Note that the stiffness of the air cushion is also not an important parameter for the design of the dancer system. The floating height of the web over the dancer, however, can be higher with the higher supply pressure which results in the higher stiffness of the air cushion. Figure 20 shows the frequency responses of the web tension to the velocity disturbance with different damping of the air cushion. Magnitudes of the resonant peaks are different; the magnitude of the peak is smaller with increasing air damping, which can be seen more easily in the phase plot than in the magnitude plot. The effect of the damping of the air cushion is also not very significant in terms of the resonant frequency of the system, but the magnitude at the resonant peak can be dramatically reduced. Note that the damping of the air cushion is an important parameter for the design of the dancer system to minimize the magnitude of the resonant peak.

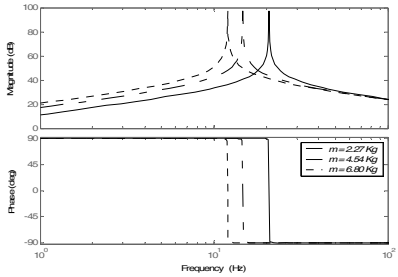

Figure 17 – Effect of effective mass of the system on frequency response of tension of web to velocity disturbance (Air dancer without air damping effect)

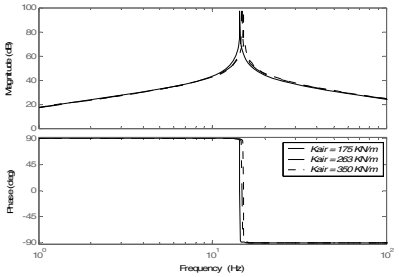

Figure 19 – Effect of the stiffness of the air cushion on frequency response of tension of web to velocity disturbance (Air dancer without air damping effect)

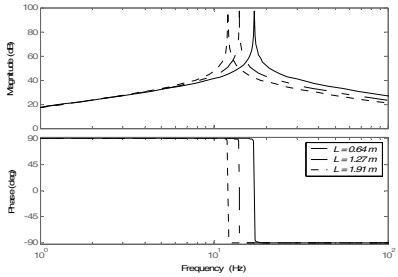

Figure 18 – Effect of length of the web span on frequency response of tension of web to velocity disturbance (Air dancer without air damping effect)

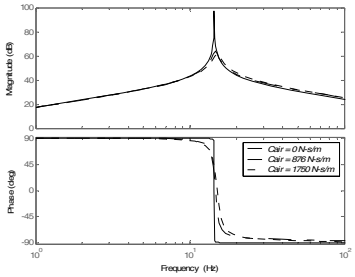

Figure 20 – Effect of the stiffness of the air damping on frequency response of tension of web to velocity disturbance (Air dancer with air damping effect)

Figure 21 shows the comparison between an air dancer and a conventional dancer, which is a typical roller having $J/MR^2 = 0.75$ as a dimensionless parameter introduced by Shelton (1997). The comparison of the frequency response of the web tension to the velocity disturbance of the web is shown in Figure 21. The air dancer and the conventional dancer (a roller) both have the resonant peak due to the translation motion of the dancer at almost the same frequency as shown in Figure 21. Note that there is another resonant peak on the curve after the first peak for the conventional dancer. This second peak is related to the rotational motion of the dancer; therefore, the second peak does not exist on the plot for the air dancer system. Note that the air dancer has a larger range of the frequency response before the resonant peak and the magnitude of the resonant peak is smaller than the magnitude the resonant peak of the conventional dancer due to the air damping effect.

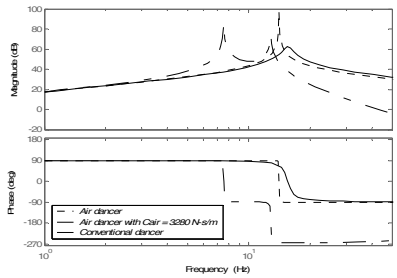

Figure 21 – Frequency response of tension of web to velocity disturbance (Comparison)

Experiments

The second stage of the experiment focused on the dynamic characteristics of the air dancer and the conventional dancer and the tension measurements in dynamic operating conditions. One of the main objectives was to measure the tension responses to the disturbance of the web velocity in magnitude and phase relationships to examine the dynamic behavior of the air dancer system compared with the conventional dancer system. The other objective was to measure the web tension using a non-contact method (from a pressure transducer) compared with the conventional tension measurement method (from a load cell).

The test setup consisted of an air-turn bar, aluminum frames (to hold the air-turn bar), a flexible web (Tyvek), a pneumatic rolling-diaphragm cylinder and instruments including two pressure transducers, a velocity sensor, two load cells, and a rotary position sensor. The air-turn bar was fabricated and installed on the vertical aluminum frames pivot-mounted on a steel rod and pillow-block bearings as shown in Figure 22. The air-turn bar was made of an 20.3 cm (8-inch) diameter polycarbonate cylinder and has air-emitting holes and a pressure tap at the center region to measure the pressure under the web as shown in Figure 23. The air-turn bar mounted on the aluminum frames was actuated as a whole by a diaphragm air cylinder (ControlAir, Model No. US-4-L). The 30.5 cm (12-inch) wide and 0.127 mm (0.005-inch) thick Tyvek material with a modulus of elasticity of 445 MPa (64,500 psi) was used as the web. A velocity disturbance system was installed in the line to generate sinusoidal velocity disturbance which resulted in sinusoidal tension disturbance on the web. It consists of two eccentric bushings to adapt a dead shaft roller, a DC motor, and 2:1 speed reduction pulleys and timing belt, an encoder, a display panel, and a speed controller. It could generate the tension disturbance with a known frequency and known amplitude independent of the web line speed. For the conventional dancer, the air turn bar was replaced with two dead shaft rollers, and other parts were kept the same as the air dancer system as shown in Figure 24. By the way, the conventional dancer was greatly improved as far as reducing the mass of the system. The original dancer was linearly actuated with a heavy steel frames and two rollers. The dancer system (air dancer or conventional dancer) was installed near the winder section in the experimental platform (donated by Rockwell Automation), which mainly consists of a web line, a number of rollers, the dancer system, unwinder and winder section (rolls), main drive roll with a nip roller for controlling the web line speed, and a web guide system for maintaining the lateral position of the web. The pictures of the platform are shown in Figure 25. The simplified sketch of the experimental platform is shown in Figure 26.

To measure the pressure under the web at the center and the plenum pressure of the air dancer system, two pressure transducers (Validyne, Model No. DP15-24) and a carrier demodulator (Validyne, Model No. CD280) were used. The pressure transducer had a maximum range of 2.22 KPa (8.9 inches of water or 0.32 psi) with a resolution 5.54 KPa (0.02225 inches of water or 0.0008 psi). The carrier yielded a DC voltage output, which was then fed into a digital data acquisition system.

A DC tachometer generator (Servo-Tek, Model No. SA-7388F-1) was used to measure the speed of the web at the downstream of the tension disturbance system and upstream of the dancer system. The velocity sensor had a range of 1000 rpm (7 V) with a 1.5 % RMS at any speed in excess of 40 RPM. The sensor yielded a DC voltage output, which was then fed into a digital data acquisition system.

To measure the tension of the web, two tension transducers (Magpower, Model No. TS150PC) and a digital tension readout (Magpower, Model No. DTR) were used. Each tension transducer had a maximum range of 667 N (150 lbf) with an accuracy of 1.11 N (0.25 lbf). The digital tension readout yielded a DC voltage output, which was then fed into a digital data acquisition system. Digital data acquisition software (LabVIEW 6) was used for collecting and storing the data. The outputs of the pressure transducers, the velocity sensor, the rotary position sensor, and the tension load cells were connected to the analog input channels of a connector (National Instruments, Model No. CB – 50 LP), which was connected to the AD converter board (National Instruments, Model No. AT-MIO-16L-9) inside the computer. The data acquisition system was configured to be in the differential mode to read all the data. It was programmed to sample 1000 data points with 12 millisecond sampling time (83.3 Hz), and the outputs were stored in text files for future analysis.

Before the test was conducted, the pressure transducers were calibrated against a vertical tube manometer that had a range of 0 to 3.74 KPa (15 inches of water). A calibration sheet for the rotary position sensor provided by the manufacturer was used. The velocity sensor was calibrated with a timer and the number of rotations of the drive roller attached the velocity sensor. The load cells were calibrated using known weights in the range of 0.0 to 49.2 N (11.05 lbf) in the compression mode with the web installed. Special care needed to be taken when calibrating the tension load cells for tension measurements in the web line because when the web was installed, there were rollers between the location of the load cells and the location where the weight is attached. Two extreme tensions were measured for each weight. In other words, the tension was measured after the rollers in-between were rotated either CW direction or CCW direction while the force was applied by the weight. While the web was running at a known web tension and speed, sinusoidal tension disturbances were generated by introducing the eccentric bushing adapters to the dead shaft roller in the web line. The frequency of the tension disturbance was increased up to 15 Hz independent of web line speed. The pressure under the web at the center region and the plenum pressure of the air dancer system were measured by the two pressure transducers, the speed of the web was measured by the velocity sensor (DC tachometer generator), the tension of the web was measured by the tension transducers (load cells), and the location of the dancer system was measured by a rotary position sensor. The values of the parameters for the analytical studies are tabulated in Table 2.

Parameter	Symbol	Value
Diameter of air-turn bar	D	20.3 cm (8 inches)
Modulus of elasticity	E	445 MPa (64,500 psi)
Mass moment of inertia	J	0.148 m-N-s^2 (1.31 in-lbf-s^2)
Length of upstream span	L_A	27.9 cm (11 inches)
Length of downstream span	L_B	87.6 cm (34.5 inches)
Effective mass of air dancer	M	4.72 kg (10.4 lbm)
Effective mass of dancer	M	19.2 kg (42.2 lbm)
Radius of dancer	R	10.2 cm (4 inches)
Radius of air-emitting holes	r	0.794 mm (1/32 inches)
Web thickness	t	0.127 mm (0.005 inches)
Web width	W	30.5 cm (12 inches)
Frequency of disturbance	f	Up to 15 Hz
Supply pressure	p_o	2.04 KPa (0.296 psig)
Web tension	T	22.2 N (5 lbf)
Web speed	V	0.236 m/s (9.3 in/s)

Table 2 – Dancer test conditions

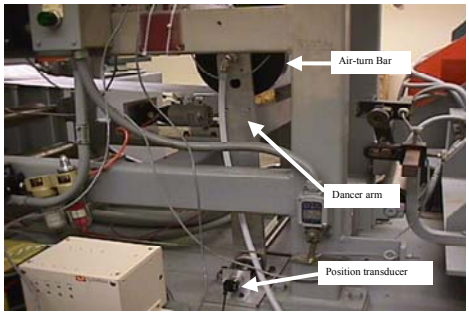

Figure 22 – Air dancer system

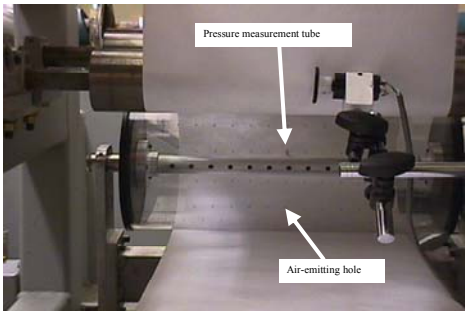

Figure 23 – Air-turn bar of the air dancer system

Figure 24 – Conventional dancer system

Figure 25 – Web line platform

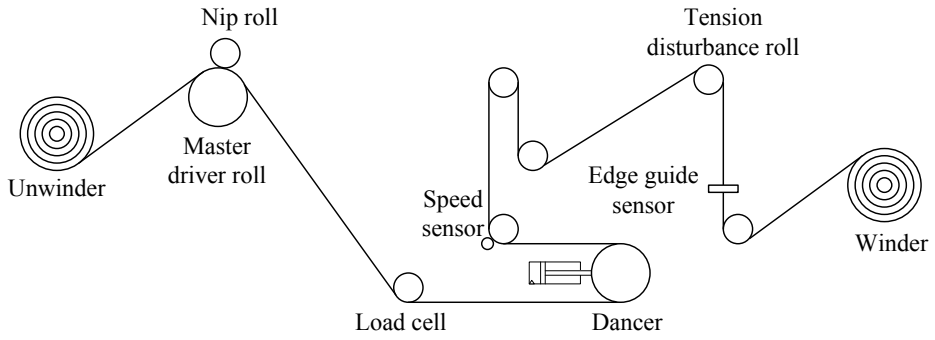

Figure 26. Sketch of experimental web line platform

The magnitude relationships of the web tension to the velocity disturbance among the web lines without the dancer, with the conventional dancer, and with the air dancer are compared in Figure 27. The magnitude relationship of the web tension to the velocity disturbance in the web line without any dancer system was about the same throughout the entire range of experiments; in other words, no resonant peak can be found in the range of testing. The resonant peaks are approximately 8.0 Hz for the web line with the conventional dancer and 11.1 Hz for the web line with the air dancer. Generally the tension was attenuated significantly by having the dancer system (either conventional or air dancer) before the resonant frequency of the system. Note that it would be much worse to have the conventional dancer system in the web line than not to have any dancer system near or after the resonant frequency of the system. For the air dancer system, however, it is better to have the air dancer system in the web line than not to have any dancer system (as an attenuator of open-loop disturbances to tension), even near or after the resonant frequency of the system. The phase relationships of the web tension to the velocity disturbance among the web lines without the dancer, with the conventional dancer, and with the air dancer were compared in Figure 28. As noticed in the magnitude relationship, no sudden change in the phase which corresponds to a resonant peak can be found in the range of tests for the web line without any dancer system. The sudden change in the phase can be found at the same frequencies as the values in the magnitude relationship, which were about 8.0 Hz for the web line with the conventional dancer and at about 11.1 Hz for the web line with the air dancer.

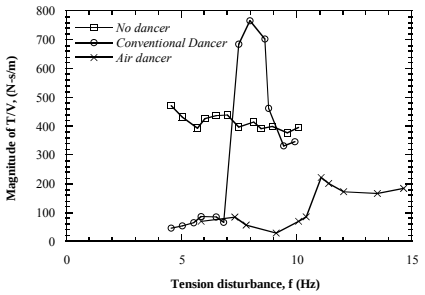

Figure 27. Magnitude relationship of tension of web to velocity disturbance

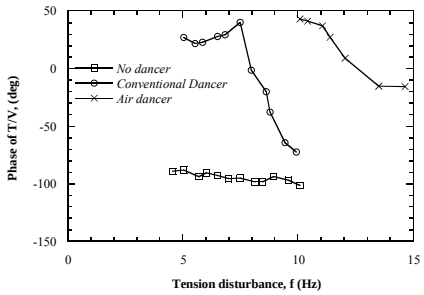

Figure 28. Phase relationship of tension of web to velocity disturbance

Comparisons

The experimental data for the magnitude relationships of the web tension to the velocity disturbance in the web lines with the conventional dancer were compared with the results from the analytical models as shown in Figure 29. Note that the simple dancer in the figure refers to the analytical model, which was derived for an ideal dancer with no rotational inertia of the dancer roller; in other words, the web was assumed to be completely slipping over the dancer roller. Comparison of the results from the analytical model with experimental data showed agreement. The resonant peak in the test, however, was not detected as high as the theoretical value from the analysis study. The analysis predicted the resonant frequency of the system at 7.7 Hz, and the simple dancer model predicted the resonant frequency of the system at 7.9 Hz. The peak from the experimental results was at about 8.0 Hz. It should also be noted that the analysis neglected mechanical damping (friction in the pivot of the dancer arm, hysteresis in the rolling diaphragm of the actuator, etc) and assumed the spring rate of the actuator to be zero. Even if a surge tank was used to avoid dynamics of the air pressure regulator and to lower the dynamic spring rate of the actuator, the mechanical spring rate is not truly zero. Even in the absence of mechanical damping in the analysis, damping is provide by the transport of strain; that is, energy enters and exits the web spans before and after the dancer in the form of strain at the dancer. The primary source of spring rate of a dancer is the spring rate of the web, which increases with EtW and decreases with length of spans at the dancer (Shelton, 1997). The experimental data for the phase relationships of the web tension to the velocity disturbance in the web lines with the conventional dancer were compared with the results from the analytical models as shown in Figure 31. The results from the analytical model agreed with experimental data even in the phase relationship. The sudden change in the phase which corresponds to a resonant peak can be found experimentally at the frequencies between 7.5 Hz and 8.0 Hz in the magnitude relationship.

The experimental data for the magnitude relationships of the web tension to the velocity disturbance in the web lines with the air dancer were compared with the results from the analytical models as shown in Figure 30. The results from the analytical model agreed with experimental data in the trend. The resonant peak in the test, however, was not detected as high as the theoretical value from the analysis study. The analysis predicted the resonant frequency of the system at 14.4 Hz. The peak from the experimental results was at about 11.1 Hz. The resonant frequencies of the system from the analytical were predicted higher than those from the experiments. The experimental data for the phase relationships of the web tension to the velocity disturbance in the web

lines with the air dancer were compared with the results from the analytical models as shown in Figure 32. The results from the analytical model agreed with experimental data even in the phase relationship. The sudden change in the phase which corresponds to a resonant peak can be found experimentally at the frequencies between 11.1 Hz and 11.4 Hz in the magnitude relationship.

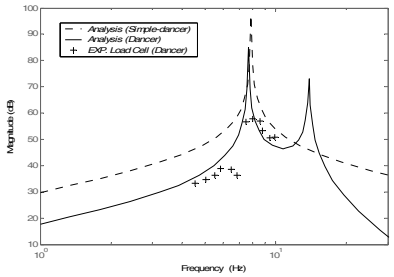

Figure 29. Comparison of magnitude relationship of tension of web to velocity disturbance (Conventional dancer)

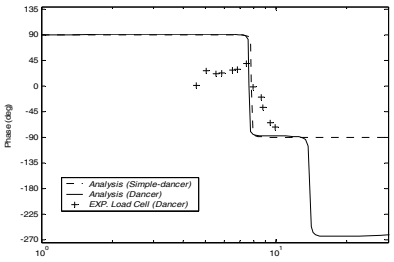

Figure 31. Comparison of phase relationship of tension of web to velocity disturbance (Conventional dancer)

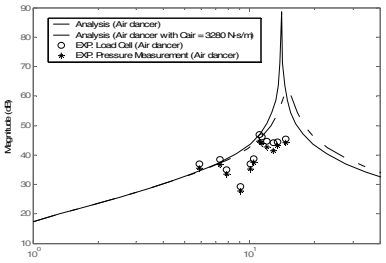

Figure 30. Comparison of magnitude relationship of tension of web to velocity disturbance (Air dancer)

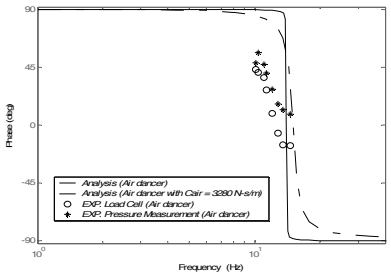

Figure 32. Comparison of magnitude relationship of tension of web to velocity disturbance (Air dancer)

CONCLUSIONS

The following conclusions can be drawn from this study:

- An aerodynamic model of air-turn bars has been developed, and the model has been experimentally verified.
- The cushion pressure profile becomes more uniform when the web tension is higher, or the supply air pressure is lower, or the web is wider.
- The size of air-emitting holes does not strongly affect the cushion pressure profile. The flotation height and the air consumption, however, dramatically increase with the size of air-emitting holes.

- The web tension based on the measured cushion pressure was within 5 % accuracy for the entire range of test conditions, up to 263 N/m (1.5 lbf/in) of web tension.
- The tension distribution on the web can be evaluated based on the pressure profile data except for the edges of the web.
- If a web is free of baggy lanes and slack edges, the web tension is proportional to the center cushion pressure of the air-turn bar under the web, and it is possible to measure the average web tension by measuring the pressure at one point.
- A dynamics model of an air dancer has been developed based on the aerodynamic model of air-turn bars.
- An air dancer becomes more efficient when its mass is small, the span over the dancer is shorter, or the supply air pressure is higher.
- Web tension and web speed do not strongly affect the resonant frequency of the system.
- Near a resonant frequency, a conventional dancer system in the web line can amplify tension fluctuations. An air dancer system, on the other hand, can significantly reduce tension variations even near its resonant frequency.
- It was shown that the air dancer system works well in the web line without any undesirable effects such as excessive lateral deflection of the web, touch-downs, and flutter.

RECOMMENDATIONS FOR DESIGN

- If a rough estimation of the supply air pressure is needed for proper operation of the air-turn bar of the air dancer, one may consider the relationship: $p_o \geq 5 \times \frac{T}{D}$
- To create a uniform flotation height and prevent touch downs at the entry and exit region where the web meets the air-turn bar of the air dancer, it is desirable to have a higher air emitting hole density in those regions.
- To minimize the effective mass of the system, it is more desirable to design a pivoted dancer system than a linearly operated dancer system.
- It is also desirable to design a dancer system with less effective mass, short span over the dancer, and higher air cushion pressure for the air dancer.
- If a rough estimation of the natural frequency of the air dancer is needed for proper operation of the dancer system in the web line, one may consider the relationship:

$$\omega_{n-air} = 2\sqrt{\frac{EtW}{\left[L_T + \pi(H_o - \frac{T}{K_{air}} + \frac{EtW}{K_{air}})\right]M}} \quad \text{for the air dancer}$$

$$\omega_n = 2\sqrt{\frac{EtW}{L_T M}} \quad \text{for the conventional dancer}$$

- As long as the web is not touching (or $T \leq \frac{3}{8} \times p_o D$), either pressure profile under the web or the center cushion pressure can be used for obtaining the web tension even in dynamic situation.

ACKNOWLEDGMENT

This research has been supported by the Web Handling Research Center at Oklahoma State University and its consortium members. The authors are grateful for their financial supports.

REFERENCES

1. Akerlund, K., Happonen, E., and Mustonen, H., "Web Tension Profile Measurement: A Tool for Runnability Control," Automation Days, Finnish Society of Automation, Helsinki, Finland, 1995, pp. 329-333.
2. Barbee, T. G., "Apparatus for Measuring Web Tension," U.S. Patent Number 3861207, 1975.
3. Blevins, R. D., Applied Fluid Dynamics Handbook, Krieger, Malabar, Florida, 1992, pp. 503.
4. Carlson, D. H., "Considerations in the Selection of a Dancer or Load Cell Based Tension Regulation Strategy," Proceedings of the Sixth International Conference on Web Handling, Stillwater, OK, 2001.
5. Chang, Y. B. and Moretti, P. M., "Aerodynamic Characteristics of Pressure-Pad Air Bars." Transactions of the ASME, Journal of Applied Mechanics, Vol. 67, No. 1, 2000, pp. 177-182.
6. Chang, Y. B., Swanson, R. P., and Moretti, P. M., "Longitudinal and Out-of-Plane Stiffness of a Web in an Air-Flotation Oven," Presented at the 1999 International Mechanical Engineering Congress and Exposition, Nashville, TN, 1999.
7. Hong, E. Y., "Aerodynamic Dancer and Tension Transducer in Web Handling", Ph. D. Thesis, Oklahoma State University, 2005.
8. Linna, H., Parola, M., and Virtanen, J., "Better Productivity by Measuring Web Tension Profile," Appita Conference, Hobart, Australia, 2001.
9. Linna, H., Moilanen, P., Mahonen, A., and Parola, M.., "Variation of the Web Tension at the Roll Change in the Printing Press," Proceedings of the Third International Conference on Web Handling, Stillwater, OK, 1995.
10. Moretti, P. M. and Chang, Y. B., "Web Flutter at Circular-Tube Air-Turn Bars," Proceedings of the Fourth International Conference on Web Handling, Stillwater, OK, 1997.
11. Muftu, S., Lewis, T. S., and Cole, K. A., "A Numerical Solution of the Euler's Equations With Nonlinear Source Terms in Modeling the Fluid Dynamics of an Air Reverser," Proceedings of the Information Storage and Processing Systems Symposium, Dallas, TX, 1997, pp. 39-48.
12. Muftu, S., et al., "A Two-Dimensional Model of the Fluid Dynamics of an Air Reverser," Transactions of the ASME, Journal of Applied Mechanics, Vol. 65, No. 1, 1998, pp. 171-177.
13. Muftu, S., "Numerical Solution of the Equations Governing the Steady State of a Thin Cylindrical Web Supported by an Air Cushion," Proceedings of the ASME Noise Control and Acoustics Division, Nashville, TN, 1999, pp. 425-434.
14. Muftu, S. and Cole, K. A., "The Fluid-Structure Interaction in Supporting a Thin Flexible Cylindrical Web With an Air Cushion," Journal of Fluids and Structures, Vol. 13, No. 6, 1999, pp. 681-708.

15. Pagilla, P. R., Perera, L. P., and Dwivedula, R. V., "The Role of Active Dancers in Tension Control of Webs," Sixth International Conference on Web Handling, Stillwater, OK, 2001.
16. Dwivedula, R. V, Zhu, Y. L., and Pagilla, P. R., "A Comparative Study on Active and Passive Dancers used for Attenuation of Web Tension Disturbances," Seventh International Conference on Web Handling, Stillwater, OK, 2003.
17. Pagilla, P. R., Dwivedula, R. V, Zhu, Y. L., and Perera, L. P., "Periodic Tension Disturbance Attenuation in Web Process Lines Using Active Dancers," Journal of Dynamic Systems, Measurement, and Control, Vol. 125, September, 2003, pp. 361-371.
18. Rajala, G. J., "Active Dancer Control for Web Handling Machine", M. S. Thesis, University of Wisconsin, 1995.
19. Reid, K. N. and Lin, K. C., "Dynamic Behavior of Dancer Subsystems in Web Transport Systems," Proceedings of the Second International Conference on Web Handling, Stillwater, OK, 1993.
20. Shelton, J. J., "Sensing of Web Tension by Means of Roller Reaction Forces," WHRC Report, Oklahoma State University, 1997.
21. Shelton, J. J., "Limitations to Sensing of Web Tension by Means of Roller Reaction Forces," Proceedings of the Fifth International Conference on Web Handling, Stillwater, OK, 1999.
22. Tang, C. C., "Computational and Experimental Study of Orifice Discharge Coefficients Affected by the presence of a Rigid Web", M. S. Thesis, Oklahoma State University, 2003.

Name & Affiliation	**Question**
Dan Carlson. 3M	If I understood your results correctly, you presented a plot that showed a conventional dancer system overlaid by the performance of the air dancer. What surprised me was that the resonant frequency of the air dancer was only slightly higher than the traditional dancer. I would have expected it to be dramatically higher.
Name & Affiliation	**Answer**
E. Hong, Oklahoma State University	The conventional dancer was a really massive system. I made it much lighter, but again, with the current conventional dancer system that I had, it was about 7 hertz. For a commercial air dancer system you could design it better than what I have. I believe that you could make an air dancer system with a much wider operating range in terms of frequency response and a better design.
Name & Affiliation	**Answer**
Y. Chang, Oklahoma State University	In an air dancer system, both the mass and the stiffness are reduced below that of a conventional dancer so that the resonant frequency may not increase significantly. The stiffness of the system is reduced because of the air cushion.
Name & Affiliation	**Question**
Tom Ungpiyakul, Kimberly-Clark Corporation	Do we know whether this has any impact on lateral dynamics?
Name & Affiliation	**Answer**
E. Hong, Oklahoma State University	It was very interesting, I was expecting a small side effect due to the air, but there was not any. The rewind web guide was located immediately after this dancer system, which was helpful. There was not much lateral misbehavior, even with several idler rolls before the web guide sensor.
Name & Affiliation	**Question**
Kee-Hyun Shin, Konkuk University	Can you guarantee the flotation height to be sufficient to prevent contact of the web?
Name & Affiliation	**Answer**
E. Hong, Oklahoma State University	If you know the web tension and the diameter of the air floatation device, then the expression I presented is a good guideline for establishing the proper operating pressure for the air floatation device. If you use this relationship, then it is almost guaranteed that the web will float over the air bar.
Name & Affiliation	**Question**
Bernd Sieber, Brueckner Maschinenbau GmbH	What is the influence of the width of the web? Do you envision problems with wider units for industrial

	applications?
Name & Affiliation	**Answer**
E. Hong, Oklahoma State University	I see no limitations for wider webs. In fact for pressure measurement purposes, you could have a better result because you have a larger region of uniform pressure profile with wider webs. It works fine for narrower webs, too.